Computational design of a high-efficiency accelerator grid for a miniature ion thruster by full-aperture ion optics simulations

Cite as: AIP Advances **9**, 035343 (2019); https://doi.org/10.1063/1.5090413
Submitted: 27 January 2019 . Accepted: 11 March 2019 . Published Online: 22 March 2019

M. Nakano, K. Nakamura, Y. Naito, Y. Nakagawa, Y. Takao, and H. Koizumi

Computational design of a high-efficiency accelerator grid for a miniature ion thruster by full-aperture ion optics simulations

Cite as: AIP Advances 9, 035343 (2019); doi: 10.1063/1.5090413
Submitted: 27 January 2019 • Accepted: 11 March 2019 •
Published Online: 22 March 2019

M. Nakano,[1,a)] K. Nakamura,[2] Y. Naito,[3] Y. Nakagawa,[4] Y. Takao,[2] and H. Koizumi[3]

AFFILIATIONS

[1]Department of Engineering, Tokyo Metropolitan College of Industrial Technology, 8-17-1, Minami-senjyu, Arakawa-ku, Tokyo 113-0852, Japan
[2]Department of Systems Integration, Yokohama National University, 79-5 Tokiwadai, Hodogaya, Yokohama 240-8501, Japan
[3]Department of Advanced Energy, The University of Tokyo, 5-1-5, Kashiwanoha, Kashiwa 277-8561, Japan
[4]Department of Aeronautics and Astronautics, The University of Tokyo, 7-3-1 Hongo, Bunkyo-ku, Tokyo 113-8656, Japan

[a)]Author to whom correspondence should be addressed. Email: mnakano@metro-cit.ac.jp

ABSTRACT

Full-aperture ion optics simulations have been conducted for the inhomogeneous plasma source of a miniature ion propulsion system (MIPS) to design a high-efficiency accelerator grid that provides high degree of the neutral confinement and absence of direct ion impingement. The designed accelerator grid has flat upstream and smoothly curved downstream surfaces with straight holes for easy low-cost manufacture. The diameter of the accelerator aperture was changed from the nominal value of 0.40 mm to 0.25 mm, which decreased neutral leakage and increased the propellant utilization efficiency from 31 to 50%. The direct impingement of ions caused by decreasing the accelerator aperture diameter was compensated by reducing the thickness of the accelerator grid while taking into account the inhomogeneous ion beam current density profile of the MIPS. An off-design performance simulation was conducted to validate the proposed grid design; the obtained results showed that the ion beam could be accelerated smoothly even during throttling the beam current between 75 and 150%. A grid wear simulation was also performed to compare the changes in the propellant utilization efficiency between the nominal and high-efficiency grids caused by erosion. It was found that the propellant utilization efficiency of the high-efficiency grid was greater than that of the nominal grid within the first 5,000 h of operation and that its lifetime exceeded 10,000 h of the accumulated operation time. By using the proposed high-efficiency accelerator grid and MIPS plasma source, the propellant utilization efficiency was increased, while the accelerator impingement current became negligible.

NOMENCLATURE

c	=	conductance
I_a	=	accelerator grid current
I_{ai}	=	direct impingement current generated in the accelerator grid
J_a	=	accelerator grid current density
J_b	=	beam current density
$m_{aperture}$	=	accelerator grid mass for the single-aperture region
$\dot{m}_{erosion}$	=	grid erosion rate for the single-aperture region
r	=	radius of the centerline aperture
t_a	=	accelerator grid thickness

Subscript

BOL	=	beginning of life
CE	=	charge exchange collision
DI	=	direct impingement
EL	=	elastic collision

I. INTRODUCTION

A gridded ion thruster is a form of electric propulsion that provides thrust by expelling high-speed ions electrostatically using a set of multi-aperture electrodes (also called grids). Propellant savings achieved by using ion thrusters are so large that high-delta V missions such as tandem GEO satellites insertions, very low altitude flights, and deep space asteroid explorations have been realized in the past two decades.[1–4] Currently, ion thrusters are employed in microspacecraft missions; for example, a miniature ion propulsion system (MIPS), which represented an electron cyclotron resonance (ECR) discharge ion thruster, was developed at the University of Tokyo and flight-tested in the PROCYON and Hodoyoshi-4 space missions.[5,6]

In gridded ion thrusters, the entire amount of propellant cannot be ionized in the discharge chamber; as a result, the unionized (neutral) propellant gas leaks through the grid apertures. In general, small propulsion systems (such as the MIPS) suffer from low propulsion performance because of the relatively large energy losses caused by their high area-to-volume ratios. Therefore, the propellant utilization efficiency (defined as the ratio of the ion beam flux to the total propellant mass flow) and the specific impulse of the MIPS are equal to around 30% and 1,200 s, respectively, which are lower than those of the typical gridded ion thrusters.

Both these parameters can be increased by improving the ion production performance in the discharge chamber and reducing the neutral leakage through the grid apertures. Various experimental and theoretical studies aimed at the improvement of the ion production in the MIPS have been conducted;[7,8] however, the present work mainly focuses on designing grid optics that decreases the amount of neutral leakage through the grid apertures.

A simple way to suppress neutral leakage is to narrow the aperture diameter of the accelerator grid; however, it also increases the probability of the direct impingement of mainstream ions that causes severe grid erosion. In the μ20 ion thruster, the initial aperture diameter of the accelerator grid was designed to be small (corresponding to an open area fraction of 9%) in order to cause direct ion impingement and ion-machined to self-determine the optimum shape of the accelerator aperture for 1,027 h of operation.[9] As a result of the ion machining process, the propellant utilization efficiency increased from 66.7 to 82.4%; however, its production cost and time were too prohibitive for micro-propulsion developers.

In the typical gridded ion thrusters, ion optics performance can be predicted with relatively high accuracy using special ion optics simulation codes.[10–24] In the MIPS, the plasma profile exhibits an inhomogeneous ring-shaped distribution due to the compact design for ECR plasma generation. Consequently, the extracted beam current and its direction are highly inhomogeneous, and the single-aperture and quarter-aperture ion optics simulations have limited applications since no appropriate symmetry boundary conditions can be applied. Therefore, full-aperture grid simulations were conducted by the authors to incorporate the inhomogeneous beam current and ion velocity distribution of the MIPS.[24] The calculated accelerator grid current and ion beam profile downstream of the thruster were in very good agreement with the experimental data. The results of full-aperture simulations show that the direct impingement of ions occurs at the downstream side of the inner barrel of the aperture in the center and periphery regions of the accelerator grid of the MIPS. It causes severe sputtering and becomes a source of spacecraft contamination. The grid material re-deposited on the grid surface forms a flake and becomes a source of electrical shortage. If this flake cannot be vaporized by electrical shortage, the further thruster operation becomes impossible. Thus, when decreasing the diameter of the accelerator grid aperture to enhance the confinement of neutrals, its shape must be changed carefully to avoid the direct impingement of ions.

Optimization of the grid shape has been conducted by several researchers.[16,19,20] The optimized grid exhibits better propulsion performance and higher lifetime; however, its shape becomes too complicated to manufacture by simple drilling and milling. This problem can be potentially solved by additive manufacturing; however, its cost is prohibitive for small organizations. The results of grid simulations conducted up to date indicate that the predicted lifetime of the grid fabricated from carbon-carbon (C/C) composite materials is greater than 20,000–30,000 h.[18,21,22] Generally, a trade-off between the grid lifetime and propulsion performance exists. In our case, the thickness of the accelerator grid can be decreased to avoid the direct impingement of ions in exchange for shortening the grid service life. Therefore, in this work, only the shape of the downstream face of the accelerator grid is changed to enable its simple machining.

The objective of this study was to design and validate an accelerator grid that would exhibit high efficiency of the neutral confinement without the direct impingement of ions within the projected lifetime and could be easily manufactured. The MIPS grid was used as an example of the grid design presented in this paper. Full-aperture ion optics and grid wear simulations were conducted to consider the highly inhomogeneous beam current and ion velocity distributions of the MIPS discharge plasma source.

II. NUMERICAL MODEL

A. Grid configuration and ion optics model

The MIPS grid system consists of two grids with 211 apertures each; the diameter of the screen grid aperture is 0.8 mm, and the thickness of the screen grid is 0.2 mm. The separation distance between the screen and the accelerator grids is 0.25 mm. In the nominal accelerator grid, the aperture diameter is 0.40 mm, and its thickness is 0.40 mm. The screen and accelerator grid voltages are equal to 1500 and −350 V, respectively. Xenon is used as the propellant, and the nominal beam current is 5.5 mA, which includes about 15% of doubly charged ions.

The numerical modeling procedure of the full-aperture simulation of the MIPS is described in a previous study.[24] The area of the simulation domain is 1/12 of that of the region with 211 apertures and hexagonal symmetry; it consists of 24 open and 11 blind apertures (see Fig. 1). The beam current density and ion velocity distributions in the discharge chamber depicted in the bottom left corner of Fig. 4 were obtained by particle in cell−Monte Carlo collision (PIC−MCC) analysis.[8] The maximum beam current is extracted from aperture #7, and the minimum beam current is extracted from aperture #21. The incident angle of ions has local minimums at apertures #1 and #7. The ion beam trajectories at apertures #7 and #21 are

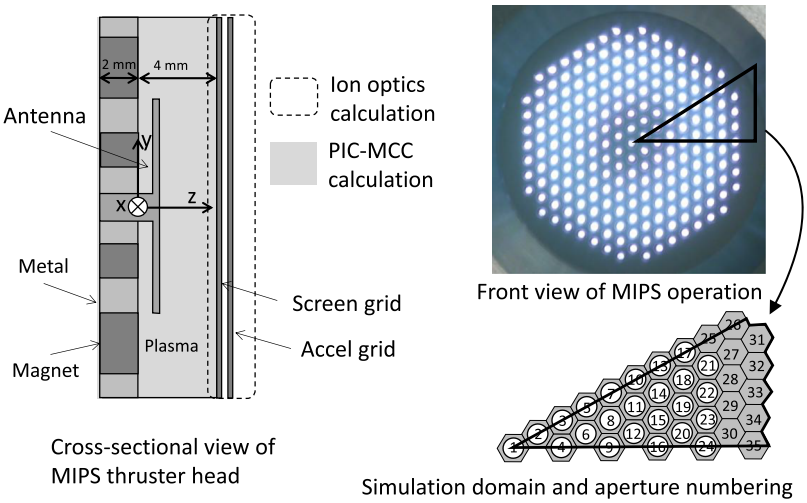

FIG. 1. Simulation domain utilized in the full-aperture analysis. The PIC-MCC calculation results served as the input of the ion optics calculations (left image). Hexagonal symmetry was used to reduce the simulation domain of 211 apertures to 24 open and 11 blind apertures (right-bottom image).

shown in Fig. 2 for reference. The extracted ion beam current of the MIPS is low, and the MIPS operates in the range near the cross-over limit. Thus, the ion beam trajectories are similar in shape. In both apertures, the crossover point is located near the upper face of the accelerator grid, and the ion beams diverge in the downstream direction. The ion beam divergence angle is slightly larger at aperture #21, and direct impingement on the inner barrel of the accelerator aperture is observed. These results are in good agreement with the relatively high accelerator grid current in the MIPS measured experimentally. They show that the utilized MIPS grid system can be further improved and optimized.

In the simulation, electrostatic potential distribution is determined by Poisson's equation using a finite element method. Singly and doubly charged ions are considered and tracked by a flux-tube method. Both charge exchange and elastic collisions between the mainstream ions and leaking neutrals were taken into account. The main computational parameters such as the boundary conditions and number of mesh divisions were determined and validated in a previous study.[24]

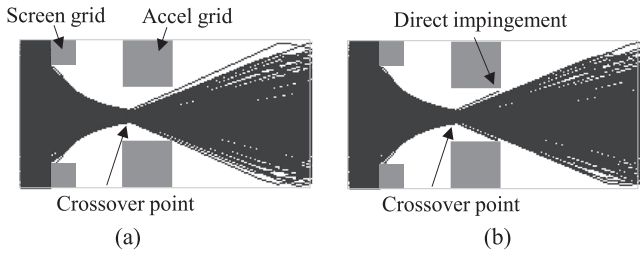

FIG. 2. Ion beam trajectories at the (a) high-current aperture #7 and (b) low-current aperture #21.

B. Grid shape optimization

Since the distance between the screen and the accelerator grids has been experimentally optimized in previous works,[5–7] only the diameter of the accelerator grid aperture and grid thickness distribution were optimized in the present study. The conductance of an orifice in the molecular regime is proportional to its area; therefore, the aperture diameter of the accelerator grid is decreased. The optimization process depicted in Fig. 3 consists of the following steps. 1) The diameter of the accelerator grid aperture is reduced as much as possible not to cause the direct impingement on the upper surface of the grid. In this process, the direct impingement on the inner barrel of the accelerator aperture is permitted (Fig. 3, middle). 2) The accelerator grid thickness of each aperture is reduced until direct impingement is no longer observed (Fig. 3, right). The grid optimized by this process is hereafter called a no-direct impingement grid.

Decreasing the accelerator grid thickness reduces the lifetime of the grid. Thus, during modeling, the index $I = \min_{1\le j\le 24} t_{a,j}/J_{b,j}$ was maximized under the constraint $\sum_{1\le j\le 24} I_{ai,j} = 0$ because, in the two-grid optics, the lifetime of the grid was determined by the structural failure in the pit and groove region, and its theoretical value was roughly proportional to $m_{aperture}/\dot{m}_{erosion} \propto t_a/J_{b,aperture}$. Although the number of open apertures has been already reduced

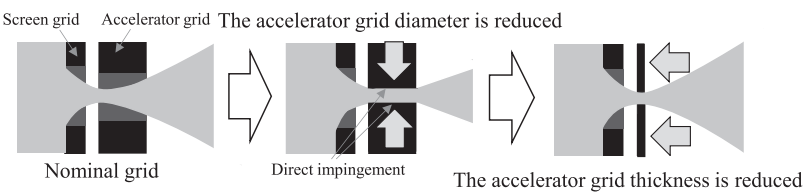

FIG. 3. A diagram illustrating the grid shape optimization process.

to 24 due to hexagonal symmetry, it was too computationally expensive to include 24 variables in the analysis. Therefore, the shape of the downstream face of the accelerator grid was approximated using two cubic functions of the radius from the centerline aperture of the accelerator grid by taking into account the shape of the beam current density distribution of the MIPS (see Fig. 4).

The shape of the cubic function is controlled by the thickness at the centerline aperture (aperture #1 at $r = 0$), thickness at the peak current density (aperture #7 at $r = r_M$), and thickness at the most distant aperture (aperture #21 at $r = r_E$) under the constraint $dt_a/dr = 0$ at $r = 0, r_M, r_E$. The thickness of the accelerator grid can be expressed as

$$t_a = \begin{cases} 2(t_a(0) - t_a(r_M))\left(\frac{r}{r_M}\right)^3 - 3(t_a(0) - t_a(r_M))\left(\frac{r}{r_M}\right)^2 + t_a(0), 0 \le r \le r_M \\ 2(t_a(r_M) - t_a(r_E))\left(\frac{r-r_M}{r_E-r_M}\right)^3 - 3(t_a(r_M) - t_a(r_E))\left(\frac{r-r_M}{r_E-r_M}\right)^2 + t_a(r_M), r_M \le r \le r_E \end{cases}.$$

In the preliminary calculations, the value of t_a/J_b tends to have minimums at apertures #1, #7, and #21. Thus, the index can be rewritten using the three control parameters $t_a(0)$, $t_a(r_M)$, and $t_a(r_E)$ as

$$I = \min(t_a(0)/J_b(0), t_a(r_M)/J_b(r_M), t_a(r_E)/J_b(r_E)),$$

which is maximized under the constraint $\sum_{1 \le j \le 24} I_{ai,j} = 0$. In these calculations, a brute-force approach was used; they were conducted for all possible combinations of $t_a(0)$, $t_a(r_M)$, and $t_a(r_E)$ by changing their values in 0.1-mm intervals.

C. Grid wear analysis

The change in the grid shape caused by erosion was taken into account using the method described in Refs. 18 and 21. The accelerator grid of the MIPS was assumed to be fabricated from a C/C composite, whose sputtering rate was evaluated by the method presented in Ref. 25. In this method, the sputtering rates of C/C composites are modeled based on Yamamura's formula[26] incorporating the shapes of carbon fibers. Model validation was performed via the ground-based endurance tests of the μ10EM, μ10PM, and μ20 ion thrusters.[18,21,27,28] For example, the experimental

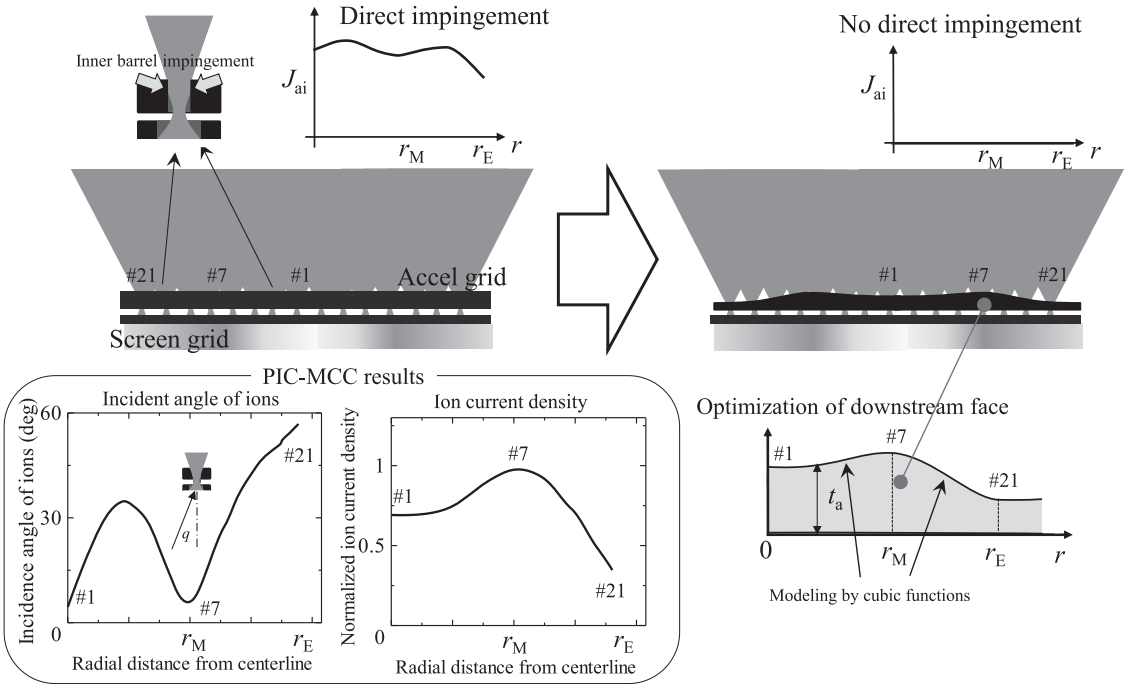

FIG. 4. Surface shape modeling of the downstream face of the accelerator grid using cubic functions.

accelerator grid current in the μ10PM ion thruster measured over the period of 0–20,000 h was 0.5±0.05 mA,[27] and its calculated value was 0.50±0.02 mA. The calculation uncertainty mainly results from the uncertainty of the sputtering rates. The experimental accelerator grid mass change after 20,000 h of operation was −0.49 g. The measurement error of the experimental data was not evaluated accurately during the endurance testing of the μ10PM ion thruster; in contrast, the estimated accelerator grid mass change during the 18,000-h endurance test of the μ10EM ion thruster varied between +0.11 g and −0.53 g.[28] The accelerator grid mass change calculated by the model was −0.39±0.10 g, which agreed with the experimental data within the uncertainties of the model. From these results, the estimated uncertainty of the accelerator grid current was 5%, and those of the grid mass change and lifetime of the accelerator grid were equal to 25%.

In this study, the MIPS was assumed to be operated in a constant beam current mode, in which the propellant mass flow rate was controlled to keep the beam current constant at a pre-determined value. The neutral mass flow rate was estimated from the conductance of the grid system determined via free molecular neutral particle calculations. Assuming that the neutral number density in the discharge chamber is fixed during operation, the neutral mass flow rate can be expressed as $\dot{m}_n = \dot{m}_{n,BOL} \times \frac{C}{C_{BOL}}$.

III. RESULTS AND DISCUSSION

A. Grid profile

First, the accelerator aperture diameter was decreased from 0.40 to 0.20 mm at a 0.05-mm interval. Figure 5 compares the direct impingement currents on the inner barrel and upstream face of the accelerator grid, indicating that the accelerator aperture diameter can be decreased to 0.25 mm without causing the direct impingement of ions on the upstream face of the accelerator grid.

Next, the following three cases were considered: (a) a nominal grid (d_a = 0.40 mm and t_a = 0.40 mm), (b) a high neutral confinement, nominal thickness grid (d_a = 0.25 mm and t_a = 0.40 mm), and (c) a high neutral confinement, no-direct impingement grid (d_a = 0.25 mm and t_a was optimized using the method described in the previous section). The downstream surface profile of grid (c) is depicted in Fig. 6 (here, the no-direct impingement profile for the nominal diameter of d_a = 0.40 mm is shown for reference). The thickness of the high neutral confinement, no-direct impingement grid is about 50% of that of the nominal grid; its inner and outer regions were depressed because the ion beams had large divergence angles and tended to impinge on the edge of the downstream side of the aperture inner barrel due to the small beam current density of the MIPS.

B. Propellant utilization efficiency, accelerator grid current, and number of sputtered atoms

Figure 7 compares the propellant utilization efficiencies of the (a) nominal, (b) high neutral confinement, nominal thickness, and (c) high neutral confinement, no-direct impingement grids. It shows that the propellant utilization efficiencies of the high neutral confinement grids are significantly increased to (b) 51% and (c) 49% from 31% obtained for of the nominal grid, respectively. In addition, a slight decrease in the propellant utilization efficiency is observed for the high neutral confinement, no-direct impingement grid since the accelerator grid thickness is reduced.

Figure 8 compares the accelerator grid currents (direct impingement current, DI, and charge exchange and elastic collision ion currents, CE+EL) for each aperture between the (a) nominal, (b) high neutral confinement, nominal thickness, and (c) high neutral confinement, no-direct impingement grids. For the nominal grid, the current due to charge exchange and the elastic collisions of ions reaches the maximum value of 5% at a radial distance of 4 mm.

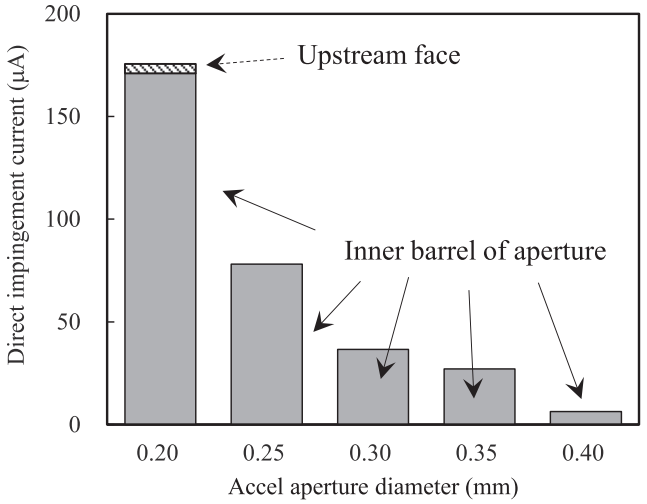

FIG. 5. Direct impingement currents generated at the upstream face and inner barrel of the aperture of the accelerator grid. At accelerator aperture diameters smaller than 0.20 mm, direct impingement occurs on the upstream face.

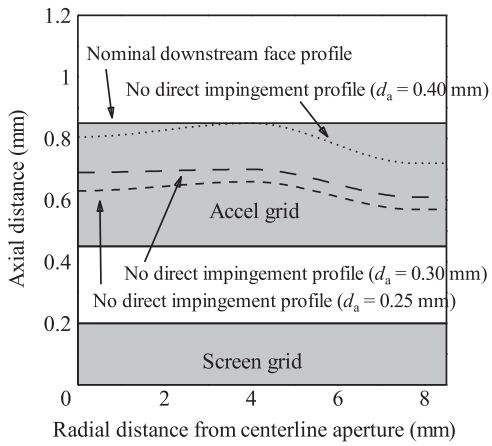

FIG. 6. Surface profiles of the nominal (solid line) and high neutral confinement (d_a = 0.25 mm), no-direct impingement (dashed line) grids. The no-direct impingement profile for d_a = 0.40 mm is added for reference (dotted line). The axial scale is magnified by a factor of 5 with respect to the radial scale for easy viewing.

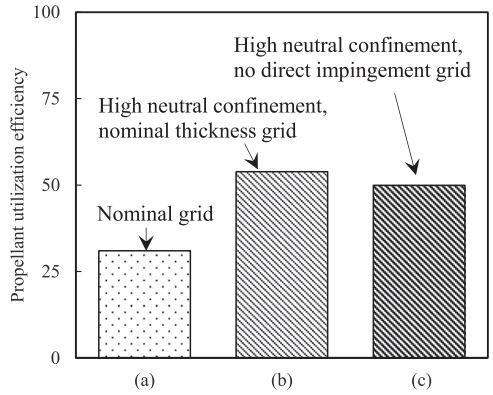

FIG. 7. Propellant utilization efficiencies of the (a) nominal (d_a = 0.40 mm, t_a = 0.40 mm), (b) high neutral confinement, nominal thickness (d_a = 0.25 mm, t_a = 0.40 mm), and (c) high neutral confinement, no-direct impingement (d_a = 0.25 mm) grids.

A small direct impingement current of less than 1% of the beam current is observed for the inner region of the grid, and a relatively large direct impingement current, which amounts to around 3% of the beam current, is obtained for the outer region of the grid. In grid (b), the currents due to charge exchange and the elastic collisions of ions were smaller with the maximum of 3%; however, the direct impingement current increased significantly to 9–15%, which completely offset the improvement of the propellant utilization efficiency (see Fig. 7). In grid (c), the direct impingement current was successfully reduced to zero, and the currents due to charge exchange and the elastic collision of ions decreased reaching the maximum value of only 2.5% at a radial position of 4 mm, which was the smallest one among grids (a)–(c).

Figure 9 compares the numbers of sputtered atoms due to the direct impingement of ions, charge exchange, and elastic collisions of ions and neutrals obtained for each aperture of the (a) nominal, (b) high neutral confinement, nominal thickness, and (c) high neutral confinement, no-direct impingement grids. Since the energies of directly impinged ions are much larger than those of the ions and neutrals generated due to charge exchange and elastic collisions, the impact of direct impingement on the grid erosion is enhanced. In grid (a), the periphery region exhibits severe sputtering due to the direct impingement of ions, which is four times stronger than the sputtering processes caused by the charge exchange and elastic collision of ions and neutrals. In grid (b), the sputtering due to direct impingement is more than ten times stronger than the processes resulting from the charge exchange and elastic collisions, which shows that the reduction in the number of directly impinged ions is essential for suppressing the grid erosion. In grid (c), the number of sputtered atoms is successfully reduced reaching the smallest value among the three grids.

C. Off-design performance

Since the high neutral confinement, no-direct impingement grid produced the optimal results under the nominal operating conditions, its off-design performance analysis was conducted. The effect of the beam current throttling was analyzed by varying the beam current between 50 and 150% of its nominal value. Figures 10(a) and (b) show the beam current profiles and incidence angles of ions obtained by PIC-MCC simulations at plasma absorption powers of 300, 500, and 700 mW, which corresponded to approximately 50%, 100%, and 150% of the nominal beam currents, respectively. Due to the similarity of the resulting curves shapes, the plasma parameters such as the beam current profile and incidence angles of ions were assumed to be close to those obtained by

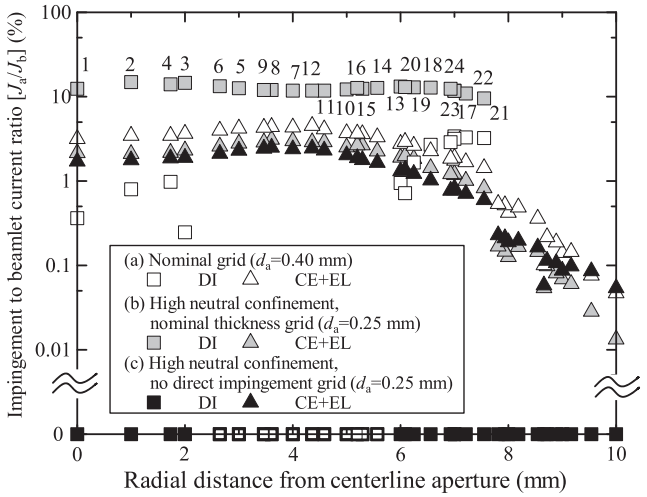

FIG. 8. DI and CE+EL accelerator grid currents obtained for each aperture of the (a) nominal (d_a = 0.40 mm, t_a = 0.40 mm), (b) high neutral confinement, nominal thickness (d_a = 0.25 mm, t_a = 0.40 mm), and (c) high neutral confinement, no-direct impingement (d_a = 0.25 mm) grids.

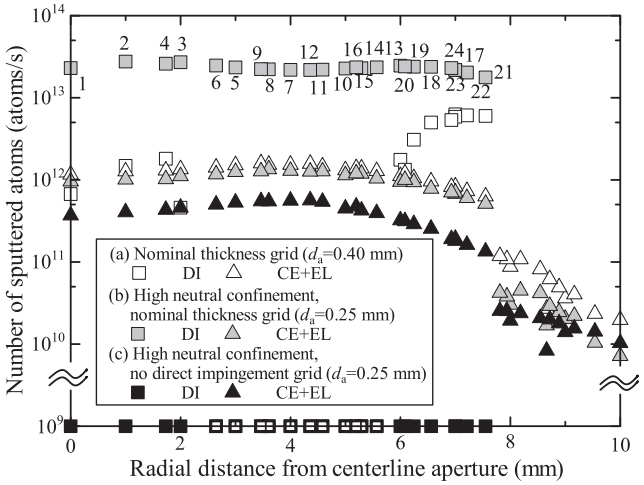

FIG. 9. Numbers of sputtered atoms due to the direct impingement of ions, charge exchange, and elastic collisions of ions and neutrals obtained for each aperture of the (a) nominal (d_a = 0.40 mm, t_a = 0.40 mm), (b) high neutral confinement, nominal thickness (d_a = 0.25 mm, t_a = 0.40 mm), and (c) high neutral confinement, no-direct impingement (d_a = 0.25 mm) grids.

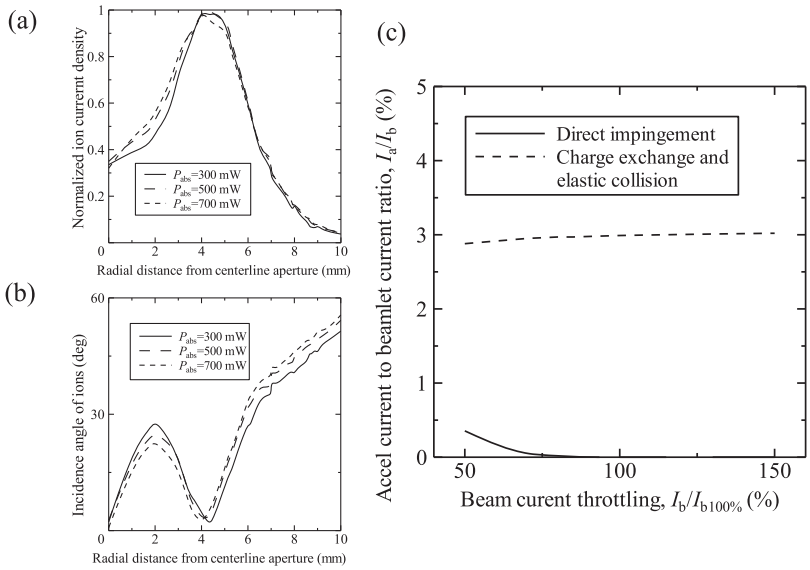

FIG. 10. (a) Ion beam profiles and (b) incident angles of ions obtained at different microwave absorption powers. (c) Effect of the beam current throttling on the DI and CE+EL accelerator grid currents.

the calculations performed at the nominal conditions. Figure 10(c) displays the ratio of the accelerator impingement current to the beam current (here, the DI and CE+EL currents are shown separately). In the throttling range between 50 and 150%, very weak direct impingement is detected at a throttling level of 50–75%, which is around 1/10 of the maximum value of the total accelerator current. No direct impingement is observed at a throttling level of 75–150%.

D. Grid wear

The endurance performance of the high neutral confinement, no-direct impingement grid was examined since the accelerator grid thickness was reduced after optimization. Figure 11 compares the changes in the propellant utilization efficiency exhibited by the nominal and high neutral confinement, no-direct impingement grids at various accumulated operating times. For reference, the changes in the aperture diameters of the accelerator grids due to erosion observed from the downstream for the nominal and high neutral confinement, no-direct impingement grids are shown in Figs. 12(a) and (b), respectively. Considering the uncertainties of the sputtering and re-deposition rates employed in the numerical model, the estimated uncertainties of the grid mass loss and grid lifetime amount to 25%.

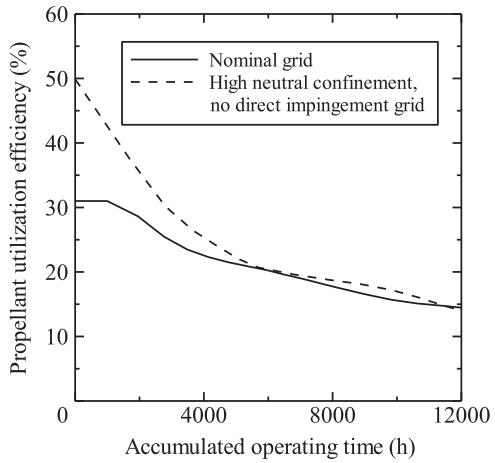

FIG. 11. Change in the propellant utilization efficiency due to grid erosion as a function of the accumulated operation time.

As indicated by Fig. 11, the difference in the propellant utilization efficiency between the nominal and high neutral confinement no-direct impingement grids is largest at the beginning of operation; it decreases gradually and becomes negligible after 5,000 h of use because their aperture diameters are almost identical (Fig. 12). Compared with the nominal grid, propellant savings can be as high as 18% at an accumulated operating time of 5,000 h and 10% at an accumulated operating time of 10,000 h.

The rightmost image in Fig. 12(b) depicts the end of life of the high neutral confinement, no-direct impingement grid caused by the structural failure at an accumulated operating time of 12,500 h. The erosion pattern containing pits and grooves is partially formed on the accelerator grid surface at an accumulated operating time of around 10,000 h, and the bridges between the innermost and adjacent apertures are completely eroded at an accumulated operating time of 12,500 h. In contrast, no structural failures were detected for the nominal grid at an accumulated operating time of 12,500 h. This relatively short lifetime of the high neutral confinement, no-direct impingement grid is a compensation for the high degree of neutral confinement and absence of direct ion impingement; however, it exhibits superior neutral confinement performance during the first 5,000 h of operation and maximum lifetime as high as 10,000 h.

E. Experimental validation

For the validation of the designed high-efficiency accelerator grid, the accelerator impingement current was measured as a

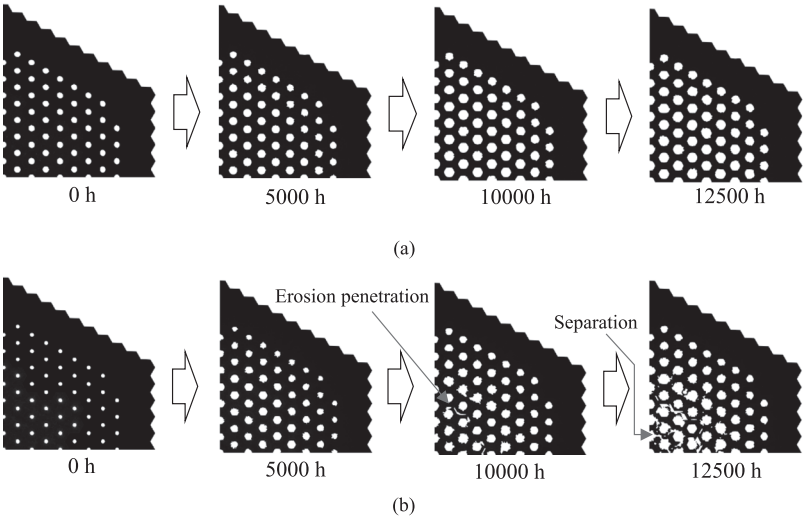

FIG. 12. Changes in the aperture diameters of the (a) nominal (d_a = 0.40 mm, t_a = 0.40 mm) and (b) high neutral confinement, no-direct impingement (d_a = 0.25 mm) grids. The bridges between the innermost and adjacent apertures in the high neutral confinement, no-direct impingement grid are completely eroded at an accumulated operating time of 12,500 h.

function of the operating time using flat (SUS304, d_a = 0.30 mm, t_a = 0.30 mm) and no-direct impingement (SUS304, d_a = 0.30 mm) grids. The aperture diameters of the grids were decreased to 0.30 mm from that of the nominal (d_a = 0.4 mm) grid to confirm that the propellant utilization efficiency could be increased by decreasing the aperture diameters of the accelerator grids. To elucidate the effect of direct impingement, the accelerator grids were made of SUS304 steel, which could be eroded relatively fast by the direct impingement of ions.

In the experiments, the MIPS discharge chamber with the 211-aperture grid set was employed as the plasma source. The beam current was set to 5.50 mA, and the screen and accelerator grid voltages were 1500 and −350 V, respectively (which were identical to those utilized in the numerical calculations). Measurements were conducted in a vacuum chamber evacuated by a turbo-molecular pump at a background pressure of 1.0×10^{-2} Pa. The accelerator impingement current was monitored for 16 h, which was equivalent to around 100 h of the operation using C/C grids because the sputtering rate of SUS304 was almost six times higher than that of C/C (SUS304 consisted of 74 wt.% Fe, 18 wt.% Cr, and 8 wt.% Ni, and the sputtering rates of Fe, Cr, Ni, and C during the Xe bombardment at 1850 eV calculated using Yamamura's formula were 3.0, 3.4, 3.0, and 0.51, respectively[26]).

Figure 13(a) shows the downstream surface profile of the no-direct impingement grid computed at d_a = 0.30 mm. A flat 211-aperture grid (d_a = 0.30 mm, t_a = 0.30 mm) was machined to follow this profile and attached to the accelerator grid position of the MIPS, whose downstream surface is photographed in Fig. 13(b). Figure 14(a) shows the change in the accelerator impingement current as a function of the accumulated operating time. After 16 h of operation, the downstream surface of the no-direct impingement grid was inspected and photographed in Fig. 14(b).

It is clearly seen that the accelerator impingement current in the no-direct-impingement grid is smaller (producing less sputtering contamination) and decreases rapidly to the steady state as compared to that in the flat grid with the same aperture diameter.

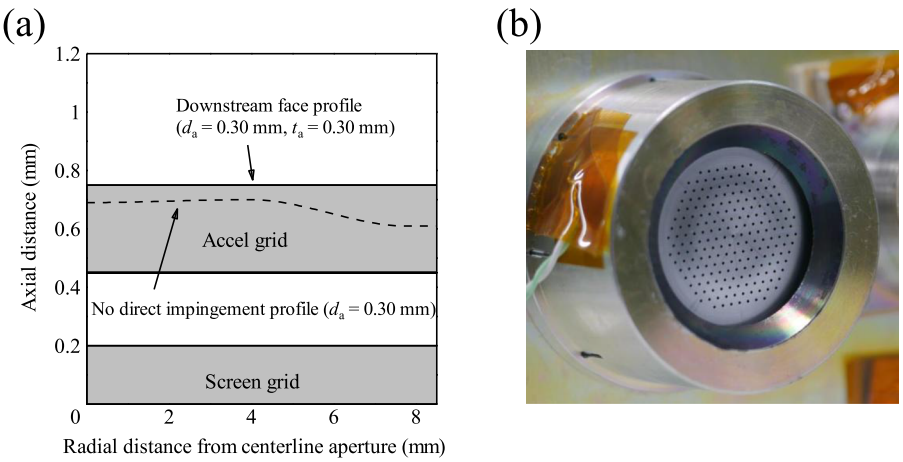

FIG. 13. (a) A computed profile of the downstream surface of the no-direct impingement (d_a = 0.30 mm) grid. (b) A photograph of the downstream surface of the no-direct impingement grid installed on the MIPS.

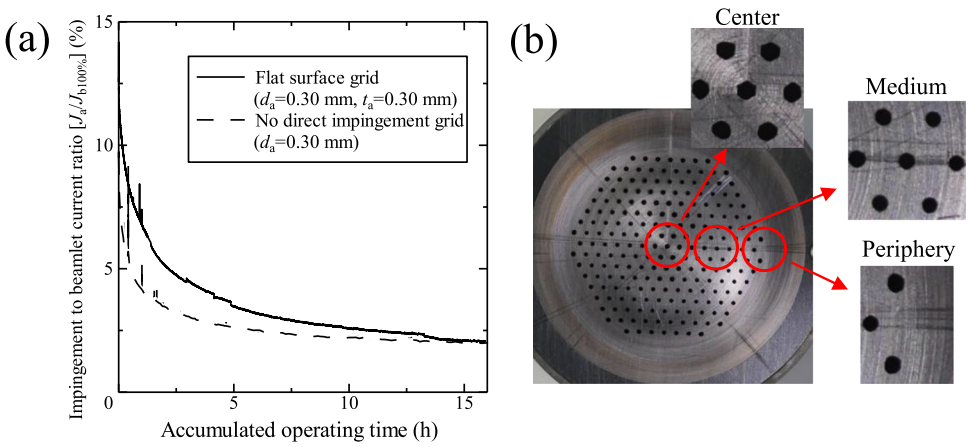

FIG. 14. (a) Accelerator impingement to beamlet current ratio as a function of the accumulated operating time. (b) Photographs of the downstream surface of the no-direct impingement grid obtained after 16 h of operation.

In Fig. 14(b), the aperture shape in the medium and peripheral regions remained almost circular after 16 h of operation, indicating that direct impingement was negligible or very small as designed; however, the central region of the grid was eroded following a hexagonal shape pattern, which was likely caused by direct impingement (typical grid erosion patterns produced by direct impingement are provided in Ref. 29). The latter is the main reason for the initial higher accelerator impingement current measured for the no-direct impingement grid in Fig. 14(a). Improvement of the modeling procedure (especially for the central region of the grid) is currently underway to enable prediction of the no-direct impingement surface profile with high precision.

In the experiment, the propellant flow rate of 16.9 μg/s was utilized to extract the beam current of 5.50±0.04 mA in the no-direct impingement grid, whereas the propellant flow rate in the nominal thickness (d_a = 0.40 mm, t_a = 0.40 mm) grid was 24.1 μg/s. The propellant flow rate was proportional-integral-derivative controlled by LabVIEW-based software using a mass flow controller calibrated within the error of ±0.98 μg/s. At these values, the calculated propellant utilization efficiency was 0.443±0.003, which was higher than the magnitude obtained for the nominal thickness grid (0.311±0.003). This enhancement resulted from the improved neutral confinement performance achieved by reducing the accelerator aperture diameter from 0.40 to 0.30 mm.

Although some improvement of the model for the prediction of the no-direct impingement surface profile is required, it is experimentally validated that the accelerator grid with high propellant utilization efficiency and no-direct impingement performance can be designed by conducting full-aperture ion-optics simulations coupled with PIC–MCC calculations for the MIPS plasma.

IV. CONCLUSIONS

A computational study was conducted to improve the propellant utilization efficiency of the MIPS by reducing the diameter of the accelerator aperture and optimizing the accelerator grid thickness distribution to prevent the direct impingement of ions from occurrence considering the inhomogeneous plasma distribution of the MIPS plasma source. This high-efficiency accelerator grid possessed the flat upstream and smoothly curved downstream surfaces with straight holes for easy low-cost manufacture. After optimization, the propellant utilization efficiency was increased from 31 to 49% at the beginning of the thruster operation. The results of off-design performance analysis showed that this ion optics could accelerate ions smoothly even during throttling the beam current between 75 and 150%.

Full-aperture grid wear simulations were performed to evaluate the grid wear. For this purpose, the change in the propellant utilization efficiency and grid surface profile were investigated as functions of the accumulated operating time. The obtained results showed that the optimized ion optics exhibited higher propellant utilization efficiency as compared to that of the nominal grid at accumulated operating times below 5,000 h and then remained at the level corresponding to the efficiency of the nominal grid until a structural failure occurred at an accumulated operating time of over 10,000 h.

The results of experimental validation showed that the high-efficiency accelerator grid possessed higher propellant utilization efficiency and smaller probability of direct impingement as compared with those of the nominal accelerator grid. Although more precise modeling of the accelerator surface is required, it was concluded that the high-efficiency accelerator grid could be designed by conducting full-aperture ion-optics simulations coupled with PIC–MCC calculations of the MIP plasma.

ACKNOWLEDGMENTS

This work was partially supported by the Grant-in-Aid for Scientific Research (S) program (grant No. 16H06370) funded by the Japan Society for the Promotion of Science.

REFERENCES

[1] C. Casaregola, in *34th International Electric Propulsion Conference* (2015), IEPC-2015-97.
[2] M. H. Corbett and C. H. Edwards, in *30th International Electric Propulsion Conference* (2007), IEPC-2007-210.
[3] H. Kuninaka, K. Nishiyama, I. Funaki, T. Yamada, Y. Shimizu, and J. Kawaguchi, J. Propul. Power **23**, 544 (2007).
[4] C. E. Garner, M. D. Rayman, and J. Brophy, in *34th International Electric Propulsion Conference* (2015), IEPC-2015-88.

[5]H. Koizumi, K. Komurasaki, J. Aoyama, and K. Yamaguchi, Trans. Jpn. Soc. Aeronaut. Space Sci. Aerosp. Technol. Jpn. **12**, Tb_19 (2014).
[6]H. Koizumi, H. Kawahara, K. Yaginuma, J. Asakawa, Y. Nakagawa, Y. Nakamura, S. Kojima, T. Matsuguma, R. Funase, J. Nakatsuka, and K. Komurasaki, Trans. Jpn. Soc. Aeronaut. Space Sci. Aerosp. Technol. Jpn. **14**, Pb_13 (2016).
[7]T. Naoi, H. Koizumi, and K. Komurasaki, Trans. Jpn. Soc. Aeronaut. Space Sci. Aerosp. Technol. Jpn. **12**, Pb_91 (2014).
[8]Y. Takao, H. Koizumi, K. Komurasaki, K. Eriguchi, and K. Ono, Plasma Sources Sci. Technol. **23**, 064004 (2014).
[9]K. Nishiyama, J. Plasma Fusion Res. Ser. **8**, 1590 (2009).
[10]Y. Arakawa and K. Ishihara, in *22nd International Electric Propulsion Conference* (1991), IEPC-91-118.
[11]Y. Hayakawa, J. Propul. Power **8**, 110 (1992).
[12]Y. Okawa, H. Takegahara, and T. Tachibana, in *27th International Electric Propulsion Conference* (2001), IEPC-01-97.
[13]J. Wang, J. Polk, J. Brophy, and I. Katz, J. Propul. Power **19**, 1192 (2003).
[14]Y. Nakayama and P. J. Wilbur, J. Propul. Power **19**, 607 (2003).
[15]R. Kafafy and J. Wang, in *41st AIAA/ASME/SAE/ASEE Joint Propulsion Conference & Exhibit* (2005), AIAA 2005-3691.
[16]C. Farnell, "Performance and lifetime simulation of ion thruster optics," Ph.D. thesis, Department of Aeronautics and Astronautics, Colorado State University, Fort Collins, Colorado, 2007.
[17]M. Tartz, E. Hartmann, and H. Neumann, Rev. Sci. Instrum. **79**, 02B905 (2008).
[18]M. Nakano, Vacuum **83**, 82 (2008).
[19]Y. Nakayama and P. J. Wilbur, in *37th Joint Propulsion Conference and Exhibit, Joint Propulsion Conferences* (2001), AIAA 2001-3786.
[20]C. C. Farnell and J. D. Williams, J. Propul. Power **26**, 125 (2010).
[21]M. Nakano, Trans. JSASS Aero. Technol. Jpn. **10**, Pb_91 (2012).
[22]M. Nakano, H. Koizumi, T. Inagaki, and K. Komuasaki, Trans. JSASS Aero. Technol. Jpn. **12**, Pb_27 (2014).
[23]A. Shagayda, V. Nikitin, and D. Tomilin, Vacuum **123**, 140 (2016).
[24]M. Nakano, K. Nakamura, Y. Nakagawa, D. Tomita, Y. Takao, and H. Koizumi, Phys. Plasmas **25**, 013524 (2018).
[25]M. Nakano, S. Hosoda, and K. Nishiyama, Trans. Japan Soc. Aero. Space Sci. **58**, 213 (2015).
[26]N. Matsunami, Y. Yamamura, Y. Itikawa, N. Itoh, Y. Kazumata, S. Miyagawa, K. Morita, R. Shimizu, and H. Tawara, IPPJ-AM-32 (1983).
[27]M. Usui and H. Kuninaka, in *30th International Electric Propulsion Conference* (2007), IEPC-2007-90.
[28]I. Funaki, H. Kuninaka, K. Toki, Y. Shimizu, K. Nishiyama, and Y. Horiuchi, J. Propul. Power **18**, 169 (2002).
[29]P. J. Wilbur, J. Miller, C. Farnell, and V. K. Rawlin, in *27th International Electric Propulsion Conference* (2001), IEPC-01-098.